



HAL
open science

3D hybrid simulations of the interaction of a magnetic cloud with a bow shock

Lucile Turc, Dominique Fontaine, Philippe Savoini, Ronan Modolo

► **To cite this version:**

Lucile Turc, Dominique Fontaine, Philippe Savoini, Ronan Modolo. 3D hybrid simulations of the interaction of a magnetic cloud with a bow shock. *Journal of Geophysical Research Space Physics*, 2015, 120 (8), pp.6133-6151. 10.1002/2015JA021318 . hal-01551990

HAL Id: hal-01551990

<https://hal.science/hal-01551990>

Submitted on 19 Jul 2020

HAL is a multi-disciplinary open access archive for the deposit and dissemination of scientific research documents, whether they are published or not. The documents may come from teaching and research institutions in France or abroad, or from public or private research centers.

L'archive ouverte pluridisciplinaire **HAL**, est destinée au dépôt et à la diffusion de documents scientifiques de niveau recherche, publiés ou non, émanant des établissements d'enseignement et de recherche français ou étrangers, des laboratoires publics ou privés.

RESEARCH ARTICLE

10.1002/2015JA021318

3D hybrid simulations of the interaction of a magnetic cloud with a bow shock

L. Turc^{1,2}, D. Fontaine¹, P. Savoini¹, and R. Modolo³

¹Laboratoire de Physique des Plasmas, UMR 7648, CNRS/Ecole Polytechnique/UPMC/Univ Paris-Sud/Obs. de Paris, Palaiseau, France, ²Now at Scientific Support Office, Directorate of Science and Robotic Exploration, European Space Research and Technology Centre (ESA/ESTEC), Noordwijk, Netherlands, ³Laboratoire Atmosphères, Milieux, Observations Spatiales, IPSL/CNRS/UVSQ/UPMC, Guyancourt, France

Key Points:

- The effects of the bow shock on magnetic clouds' magnetic field is investigated
- The extent of the alteration of the MC's structure depends on the encountered shock configuration
- The magnetic cloud causes an attenuation of the foreshock

Correspondence to:

L. Turc,
lucile.turc@esa.int

Citation:

Turc, L., D. Fontaine, P. Savoini, and R. Modolo (2015), 3D hybrid simulations of the interaction of a magnetic cloud with a bow shock, *J. Geophys. Res. Space Physics*, 120, 6133–6151, doi:10.1002/2015JA021318.

Received 10 APR 2015

Accepted 25 JUL 2015

Accepted article online 31 JUL 2015

Published online 25 AUG 2015

Abstract In this paper, we investigate the interaction of a magnetic cloud (MC) with a planetary bow shock using hybrid simulations. It is the first time to our knowledge that this interaction is studied using kinetic simulations which include self-consistently both the ion foreshock and the shock wave dynamics. We show that when the shock is in a quasi-perpendicular configuration, the MC's magnetic structure in the magnetosheath remains similar to that in the solar wind, whereas it is strongly altered downstream of a quasi-parallel shock. The latter can result in a reversal of the magnetic field north-south component in some parts of the magnetosheath. We also investigate how the MC affects in turn the outer parts of the planetary environment, i.e., from the foreshock to the magnetopause. We find the following: (i) The decrease of the Alfvén Mach number at the MC's arrival causes an attenuation of the foreshock region because of the weakening of the bow shock. (ii) The foreshock moves along the bow shock's surface, following the rotation of the MC's magnetic field. (iii) Owing to the low plasma beta, asymmetric flows arise inside the magnetosheath, due to the magnetic tension force which accelerates the particles in some parts of the magnetosheath and slows them down in others. (iv) The quasi-parallel region forms a depression in the shock's surface. Other deformations of the magnetopause and the bow shock are also highlighted. All these effects can contribute to significantly modify the solar wind/magnetosphere coupling during MC events.

1. Introduction

Interplanetary coronal mass ejections (ICMEs) are large-scale solar wind transients associated to huge eruptions in the solar corona, the so-called coronal mass ejections (CMEs). When directed earthward, ICMEs often drive intense magnetic activity in the terrestrial magnetosphere and thus play a central role in space weather at Earth. Magnetic clouds (MCs) are a subset of ICMEs characterized by a specific flux rope-like structure, which have been shown to be particularly geoeffective [e.g., *Echer et al.*, 2008a, 2008b; *Yermolaev et al.*, 2012]. As first defined by *Burlaga et al.* [1981], MCs are identified by an enhanced magnetic field which rotates smoothly over a large angle, accompanied by a depressed proton temperature. MCs are large-scale structures: the smooth rotation of their magnetic field unfolds over time intervals ranging from several hours to several days [*Lepping et al.*, 2006].

In order to predict their near-Earth's consequences, considerable effort has been made over the last decades to find correlations between the MCs' properties in the upstream solar wind and the level of disturbances they induce in the magnetosphere [*Zhang et al.*, 2004; *Huttunen et al.*, 2005; *Echer et al.*, 2005; *Gopalswamy et al.*, 2008; *Kilpua et al.*, 2012]. These statistical studies reveal that the presence of southward magnetic fields inside the MC generally leads to the development of a geomagnetic storm. However, in some cases, this relationship is not straightforward. For example, it has been shown that a substantial fraction of MCs with southward fields does not trigger significant magnetospheric activity [e.g., *Zhang et al.*, 2004; *Huttunen et al.*, 2005; *Gopalswamy et al.*, 2008]. Therefore, to further our understanding of MCs' geoeffectivity, it is necessary to examine in more detail their interaction with the terrestrial environment.

When MCs arrive in the vicinity of Earth, they first encounter the bow shock, which slows down the incoming supermagnetosonic flow to submagnetosonic speeds. Then they propagate into the region of shocked plasma called the magnetosheath, before impinging on the magnetopause. The magnetosheath acts as an interface between the solar wind and the magnetosphere and mediates the energy transfer from the former

to the latter. It is also the magnetosheath magnetic field which ultimately reconnects with the Earth's magnetic field. A number of recent studies [Lavraud and Borovsky, 2008; Šafránková et al., 2009; Lopez et al., 2011; Farrugia et al., 2013; Turc et al., 2014a, 2014b] suggest that the bow shock and the magnetosheath may play a key role in the solar wind-magnetosphere interaction during MC events, which is generally overlooked.

Owing to their enhanced magnetic field, which is often accompanied by a depressed proton density, the Alfvén Mach number M_A is usually lower during MCs than in the quiet solar wind, and the plasma β , ratio between the thermal and magnetic pressures, drops frequently below 1. When such conditions prevail, the magnetic forces are expected to dominate the dynamics of the magnetosheath, giving rise to a number of unusual features that could influence the solar wind/magnetosphere coupling, as detailed for example in Lavraud and Borovsky [2008]. In particular, enhanced flows exceeding the solar wind speed can arise in the nightside magnetosheath, near the flank magnetopause [Rosenqvist et al., 2007; Lavraud et al., 2007; Fairfield et al., 2007; Lavraud and Borovsky, 2008; Erkaev et al., 2011, 2012; Farrugia et al., 2013; Lavraud et al., 2013]. Their location depends on the orientation of the upstream magnetic field [Lavraud et al., 2013]. Also, the plasma depletion layer is particularly extended and could thus control to a large extent how energy and momentum are transferred through the magnetopause [Farrugia et al., 1995, 2013]. In addition, the low M_A alters the bow shock compression ratio, which becomes much more sensitive to modest variations in the upstream solar wind parameters [Lopez et al., 2004, 2011]. More importantly, Lopez et al. [2011] show that the near-Earth current system can be profoundly modified during low M_A conditions, and, as a consequence, the solar wind energy transferred to the magnetosphere would be primarily extracted at the bow shock.

On the other hand, the bow shock alters in return the properties of MCs. It can in particular modify their magnetic structure, as shown for example in Turc et al. [2014a] with a magnetosheath model and Turc et al. [2014b] using spacecraft observations. The extent of this alteration depends on the local geometry of the shock. It becomes significant when the shock configuration turns quasi-parallel, i.e., when the normal to its surface becomes nearly parallel to the upstream magnetic field. In this case, deviations of up to 60° have been observed between the magnetic field orientation in the solar wind and in the magnetosheath.

The aim of the present work is to investigate the consequences of the bow shock's crossing on the magnetic structure of MCs by the means of hybrid simulations. To our knowledge, previous numerical studies of the interaction of MCs with the Earth's environment have all been conducted on magnetohydrodynamic (MHD) simulations and focus primarily on the effects of MCs inside the magnetosphere [e.g., Goodrich et al., 1998; Lopez et al., 2000, 2001; Luhmann et al., 2004]. A number of works [e.g., Yan and Lee, 1996; Šafránková et al., 2007; Němeček et al., 2011, and references therein] also investigate the impact on the terrestrial bow shock of interplanetary shocks, which can be associated to MCs, with a primary interest in waves, instabilities, and discontinuities generated by this interaction. In the present study, however, we focus on the inner part of the MC, characterized by their enhanced and slowly rotating magnetic field, and not on the discontinuities that may precede it and would result in a completely different type of interaction. In the case studied here, the bow shock experiences a slow rotation of the upstream magnetic field as the MC passes by, which can be considered as a succession of quasi-stationary states.

Numerical simulations of the MC/bow shock interaction will provide us with the global context unattainable with localized spacecraft observations such as those reported by Turc et al. [2014b]. Also, in contrast to the Turc et al. [2014a] semianalytical model, the response of the planetary environment to the slowly changing upstream parameters, as well as the alteration of the MC across the bow shock, are self-consistently derived from basic equations in numerical simulations. Therefore, we will be able to investigate how the MC affects the outer parts of the planetary environment, from the bow shock to the magnetopause, and how the energy is distributed inside the magnetosheath. In addition, the use of the hybrid formalism will allow us to examine the quasi-parallel region of the bow shock, and in particular its associated ion foreshock.

The simulation code used in this work and its adaptation to the purpose of this study are presented in section 2. In sections 3 and 4 we describe the results of two simulation runs, corresponding to two different MCs leading to a different interaction with the bow shock. Section 5 concludes this paper with a summary and a discussion.

2. Simulation Model

The hybrid approach treats the electrons as a fluid but retains the ion dynamics and thus offers a trade-off between fully kinetic and magnetohydrodynamic (MHD) simulations. This formalism is employed for two main reasons. First, the quasi-parallel shock configuration, which is of particular importance in the interaction of MCs with the bow shock [Turc *et al.*, 2014a, 2014b], is a highly complex region where the ion dynamics play a paramount role. Therefore, the fluid description of the plasma is not sufficient to capture all the features associated with this shock regime and especially the development of the foreshock region upstream of the quasi-parallel bow shock. Second, the problem that is addressed here is essentially three-dimensional in nature, as the MC's magnetic field can rotate in a nonplanar fashion and assume any orientation. Also, we want to investigate the large-scale phenomena taking place inside the magnetosheath. Our study thus requires a 3-D global simulation, which rules out a full particle treatment; hence, our choice of hybrid simulations.

This work is based on the parallel hybrid code developed by Modolo *et al.* [2005] which describes the interaction of the solar wind with a planetary environment. Initially designed for martian studies [Modolo *et al.*, 2005, 2006], this model has been adapted since then to various solar system bodies, such as Titan [Modolo and Chanteur, 2008], Mercury [Richer *et al.*, 2012], or Ganymede (L. Leclercq *et al.*, 3D magnetospheric parallel hybrid multi-grid approach applied to planetary space physics, submitted to *Journal of Computational Physics*, 2015, hereinafter referred to as L. Leclercq *et al.*, submitted manuscript, 2015). We adapt it to describe the interaction of an MC with the terrestrial bow shock.

In hybrid simulations, the ions are described by macroparticles whose dynamics are determined from the equations of motion as if they were physical charged particles, whereas the electrons are considered as a massless fluid ensuring the charge neutrality of the plasma. The electronic fluid contributes to the total pressure and the currents, and electrons are assumed to behave adiabatically in our simulations. In the code we use, the system of equations controlling the time evolution of the electromagnetic fields and the motion of the particles is solved using the Current Advance Method and Cyclic Leapfrog (CAM-CL) algorithm [Matthews, 1994]. Moments are computed from particle deposition on the simulation grid using a Cloud-In-Cell approach [Birdsall and Langdon, 1985]. It is a standard procedure to determine moments from particle-in-cell models. At each time step moments and magnetic field are smoothed to limit numerical noise (L. Leclercq *et al.*, submitted manuscript, 2015).

The coordinate system which will be used throughout this paper is defined as follows: its origin is set at the center of the obstacle, i.e., the Earth, with the x axis pointing sunward; the incoming solar wind flows along the $-x$ direction. The z axis is parallel to the planetary dipole's axis, and y completes the right-handed triple. Open boundary conditions are used in the x direction, on the entry and exit faces, while periodic conditions are applied along the y and z directions, transverse to the solar wind flow.

2.1. Planetary Environment

In this study, we do not reproduce the terrestrial environment in its actual dimensions, which would require the simulation to be run on tens of thousands of cores [Karimabadi *et al.*, 2011], but we create a planetary environment whose characteristics mimic Earth's at a smaller scale, as is generally done in hybrid simulations [e.g. Omidi *et al.*, 2005; Blanco-Cano *et al.*, 2006; Omidi *et al.*, 2014; Karimabadi *et al.*, 2014, and references therein]. Note that neither the ionospheric nor the magnetospheric plasma are included in our simulations. However, since we focus on the outer parts of the planetary environment, from the foreshock to the magnetopause, this should not affect our results. More precisely, we set the intensity of the dipole moment so that the curvature of the bow shock and the magnetopause, relative to the size of the magnetic obstacle, are close to those observed at Earth for similar incoming solar wind parameters. The reduced computational cost of our simulations allows us to investigate how different orientations of the MC's magnetic field influence its interaction with the bow shock, while keeping unchanged the main features of this interaction. Additional constraints are that the flanks of the bow shock must not reach the lateral faces of the simulation domain because of the periodic boundary conditions along y and z , and that the magnetosheath must be large enough, i.e., a width of at least several grid cells, to allow for investigation of the MC's structure in this region.

The simulation box used in this work is a 3-D uniform cartesian grid with a spatial resolution of $1 c/\omega_{pi}$ (ion inertial length in the undisturbed solar wind, where c is the speed of light and ω_{pi} the ion plasma frequency), as used for example in Omidi *et al.* [2013, 2014] and in one of the runs presented in Karimabadi *et al.* [2014]. The simulation domain comprises $200 \times 550 \times 550$ cells, along x , y , and z respectively, and each of them contains

10 particles at the beginning of the simulation. The distribution of the cells along the different directions is chosen to match the geometry of the simulated environment, namely, the large flaring of the bow shock.

The dipole moment is set to $\mu = 8.10^{11} \mu\text{T} \cdot \text{m}^3$. The relative shapes of the magnetopause and the bow shock are compared to those found at Earth for similar solar wind conditions. The *Shue et al.* [1998] and the *Jeřáb et al.* [2005] models are taken as references for the magnetopause and bow shock shapes, respectively, as was done in previous MC studies [*Turc et al.*, 2013, 2014a]. For each boundary, we compare the ratio between the geocentric distances at the terminator and at the subsolar point in the simulation and in the models and we find a good agreement. According to the study by *Omidi et al.* [2004], if the distance of the magnetopause subsolar point from the center of the obstacle exceeds $20 c/\omega_{pi}$, the structure of the magnetosphere should be similar to that of Earth. In our simulation, the magnetopause nose is located at around $25 c/\omega_{pi}$ from the center of the obstacle, which is above the threshold set by *Omidi et al.* [2004]. Therefore, the structure of the terrestrial magnetosphere should be correctly reproduced in our smaller-scale magnetosphere. Also, the basic processes taking place at the shock should resemble those observed at Earth [*Omidi et al.*, 2005].

The subsolar point of the terrestrial magnetopause is found on average at around $640 c/\omega_{pi}$ from the Earth's center. The simulated magnetosphere is thus 26 times smaller than the actual magnetosphere. A similar scaling factor, about 20, is also obtained for the magnetosheath width at the subsolar point. The slight difference between these two scaling factors is probably due to the fact that the bow shock standoff distance not only depends on the size of the obstacle but also on its shape [e.g., *Farris and Russell*, 1994] which varies with the dipole strength. This implies that the transit time inside the simulated magnetosheath is roughly 20 times shorter than in reality, of the order of 10 s instead of a few minutes. The small size of the simulated magnetosheath will most likely affect the development of some types of waves inside this region. For instance, because of the short transit time, the modes with a rather low growth rate may not have time to develop before reaching the magnetopause. Similarly, in the foreshock, a larger system would allow more time for waves to evolve and steepen and more space for wave-particle interactions to occur.

The total number of particles in our simulations is relatively high, 605×10^6 particles, compared for example to the 60×10^6 particles used by *Omidi et al.* [2013] in 2-D simulations or to the 300×10^6 used by *Lin and Wang* [2005] in 3-D simulations. As concerns the number of particles per cell (N_{ppc}), there are very large disparities in published works: it ranges from a few [*Modolo et al.*, 2005] to a few tens [*Omidi et al.*, 2005; *Blanco-Cano et al.*, 2006; *Omidi et al.*, 2013] and up to several hundreds of particles [*Lin and Wang*, 2005; *Karimabadi et al.*, 2014]. In our case, the N_{ppc} is in the lower part of this distribution despite the large total number of particles because our simulation domain is 3-D and comprises a rather large number of cells in all three directions. It remains nevertheless acceptable, and the code we are using is robust enough to accommodate small N_{ppc} [*Modolo et al.*, 2005]. This rather low N_{ppc} could result in an imprecise description of the high-energy tail of the ion distribution, due for instance to acceleration at the bow shock, because of the lack of statistics. However, as will be shown later, it is sufficient to describe the processes of interest here, namely, the global features and the wave properties of the foreshock and allows us to perform 3-D global simulations of a planetary environment.

2.2. Simulating the Magnetic Cloud

As our main interest lies in the magnetic structure of MCs, i.e., their enhanced and smoothly-rotating magnetic field, all the other solar wind parameters (density, velocity, and temperature) will be kept constant throughout the simulation. Therefore, we will not model the shock nor the sheath which often precede MCs but only their inner part which can be described by a flux rope [*Burlaga*, 1988]. This allows us to disentangle the effects of the MC proper from those due to its sheath, which are known to drive different types of activity in the Earth's magnetosphere [*Huttunen et al.*, 2002; *Huttunen and Koskinen*, 2004]. The ion density is set to 6 cm^{-3} and the bulk flow velocity to $500 \text{ km} \cdot \text{s}^{-1}$. The initial Alfvén Mach number is equal to 5.6 and the plasma β to 0.32.

To describe the MC's magnetic structure, a time-varying interplanetary magnetic field is imposed on the entry face of the simulation, which is then convected by the solar wind flow across the simulation domain. Since MCs are huge structures compared to the size of the Earth's environment [e.g., *Lepping et al.*, 2006], we neglect their curvature, and thus, the same magnetic field is applied to all the cells of the entry face at a given time. Note that in order to ensure that the magnetic field remains divergence free at the boundary, its B_x component cannot be modified in the course of the simulation. The rotation of the magnetic field will then necessarily be performed in the YZ plane. This also implies that the increase of the magnetic field magnitude will only affect the B_y and B_z components.

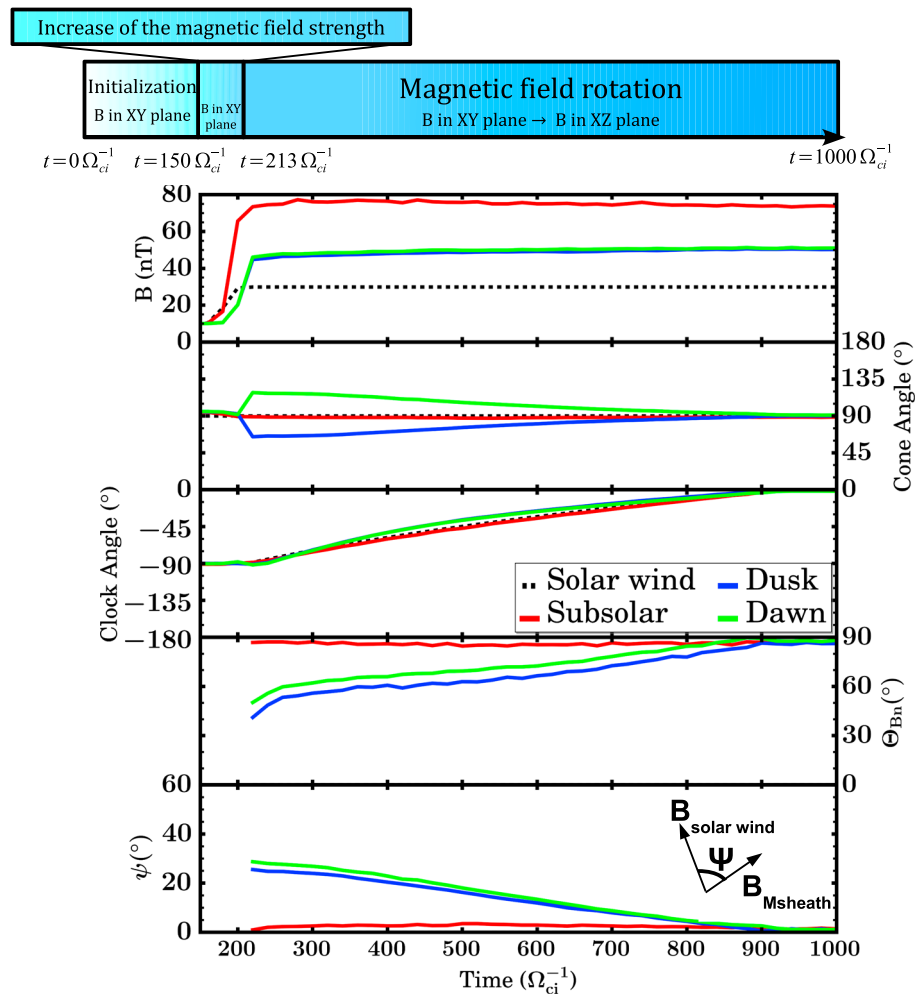


Figure 1. Observations from virtual spacecraft inside the magnetosheath (red: in the subsolar region; green: in the dawn flank; blue: in the dusk flank) and input magnetic field at the entry of the simulation domain (black). (first to fifth panels) Magnetic field magnitude, cone angle, clock angle, Θ_{Bn} encountered upon entering the magnetosheath, and the angle ψ between the magnetic field in the solar wind and in the magnetosheath.

The simulation is divided into three phases, which are schematized in the upper part of Figure 1 and are defined as follows:

Step 1. From $t = 0$ to $t = 150 \Omega_{ci}^{-1}$, where Ω_{ci} is the proton gyrofrequency, the magnetic field lies in the equatorial plane, with a given angle between B_x and B_y , and its intensity is set to a constant $B = 10$ nT. In this initialization phase, the magnetosphere and the bow shock form from the interaction of the dipolar field with the incoming solar wind and reach a steady state.

Step 2. From $t = 150 \Omega_{ci}^{-1}$ to $t = 213 \Omega_{ci}^{-1}$, the magnitude of the B_y component is increased from B_{y0} to $3B_{y0}$, following a hyperbolic tangent. The B_x component remains unchanged. The enhancement of the magnetic field strength spans $10\tau_{ci} \approx 63 \Omega_{ci}^{-1}$, where τ_{ci} is the ion gyroperiod, to give time to the ions to adapt to the changing magnetic field. Note that if $B_x \neq 0$ this will modify the magnetic field direction. The duration of Step 2 is about 1 min in real time, which corresponds to the time scale of the increase of the magnetic field strength observed at an MC's arrival.

Step 3. From $t = 213 \Omega_{ci}^{-1}$ to $t = 1000 \Omega_{ci}^{-1}$, we perform a 90° rotation of the magnetic field direction about the x axis. The magnetic field then rotates from the XY to the XZ plane. When the B_x component is negligible, the time-varying magnetic field follows the flux rope model of *Burlaga* [1988] which is based on Bessel's functions. In order to separate the effects of the changes in the magnetic field strength and direction, the magnetic field

magnitude is kept constant during this third phase. The duration of the MC, scaled to the transit time in our simulation domain, is consistent with that of an MC passing by the Earth's magnetosphere.

In Step 3, we only model the first half of an MC, since the simulation ends when the magnetic field lies in the XZ plane. In the second part of the event, the magnetic field direction would rotate back into the XY plane, pointing this time in the opposite direction along the y axis. This would lead to a similar interaction as in Step 3, mirrored relative to the XZ plane because of the change of sign of the B_y component. The transit time inside the simulation domain is $36 \Omega_{ci}^{-1}$, which is much shorter than the duration of Step 3. Therefore, the rotation of the MC's magnetic field is slow enough to be considered as a succession of quasi-stationary states. The total duration of the simulation is $1000 \Omega_{ci}^{-1}$, and the chosen time step is $0.05 \Omega_{ci}^{-1}$. In this paper, we will discuss two simulations, corresponding to two orientations of the magnetic field direction and thus to a different configuration at the bow shock.

3. Simulation 1: Magnetic Cloud With a Negligible B_x Component

In the first simulation described in this paper, hereafter referred to as Simulation 1, we choose an orientation of the MC's magnetic field which is similar to one of the cases examined by *Turc et al.* [2014a]. As this MC configuration leads to a rather simple interaction with the bow shock, i.e., to a mostly quasi-perpendicular geometry, the results we obtain with the hybrid code can be directly compared to previous modeling and observational studies carried out in the Earth's environment for similar conditions [*Turc et al.*, 2014a, 2014b]. The value of the angle between the magnetic field and the flow direction, the so-called cone angle, is set to 85° . The B_x component is thus negligible during the entire simulation, so that the entire dayside bow shock is in a quasi-perpendicular geometry. At the beginning of the run, the magnetic field is aligned with the y direction, and $|B_y| = 10$ nT. In Step 2, it increases to 30 nT, causing the M_A to decrease to 1.8 and the upstream plasma β to 0.036. Then in Step 3 the magnetic field rotates from the y to the z direction.

3.1. Alteration of the MC's Structure

Similarly to what was done in *Turc et al.* [2014a], we use virtual spacecraft located in different regions of the equatorial magnetosheath to investigate the evolution of the magnetic field downstream of the bow shock as the MC passes by. The red curves in Figure 1 correspond to the subsolar region (spacecraft position: $x = 40 c/\omega_{pi}$, $y = 0$, $z = 0$), while the green and blue spacecraft probe the dawn ($x = 0$, $y = -80 c/\omega_{pi}$, $z = 0$) and dusk ($x = 0$, $y = 80 c/\omega_{pi}$, $z = 0$) side magnetosheath, respectively, in the terminator plane ($x = 0$). The magnetic field in the solar wind is drawn in black dashed curves. The interval displayed in Figure 1 excludes the initialization phase, which is not relevant for our study, and thus ranges from $t = 150 \Omega_{ci}^{-1}$ to $t = 1000 \Omega_{ci}^{-1}$.

The first panel of Figure 1 shows that the three virtual spacecraft in the magnetosheath encounter an enhanced magnetic field, compared to that in the upstream solar wind, due to the expected magnetic compression caused by the bow shock's crossing. Owing to the piling up of the field lines, the magnetic field strength is highest in the subsolar region (red curve). The slight delay between the increase of the magnetic field magnitude in the solar wind (black dashed curve) and in the magnetosheath (blue, green, and red curves) is due to the fact that it takes about $20 \Omega_{ci}^{-1}$ for the solar wind to propagate from the entry of the simulation domain to the terminator plane.

The magnetic field cone angle (second panel of Figure 1) remains roughly unchanged in the subsolar magnetosheath (red curve) but varies by up to 30° on the flanks of the magnetosheath at the beginning of the MC, either increasing (dawn side, green curve) or decreasing (dusk side, blue curve). The direction of variation of the cone angle on either sides of the magnetosheath is consistent with the draping of the field lines around the magnetosphere. As time progresses, the cone angle returns gradually to a value similar to that in the solar wind because of the rotation of the upstream magnetic field from the y to the z direction. At the end of the simulation, the draping no longer alters the orientation of the magnetic field lines in the equatorial plane. The third panel of Figure 1 shows the magnetic field clock angle, i.e., the polar angle of the magnetic field in the YZ plane relative to the z axis. In the solar wind (black dashed curve), the clock angle increases from -90° to 0° as the magnetic field rotates from the XY to the XZ plane. The same rotation is observed in the magnetosheath (solid curves), with only minor discrepancies on the flanks (green and blue curves).

In the fourth panel of Figure 1 are displayed the values of Θ_{Bn} , the angle between the normal to the bow shock, and the upstream magnetic field. To determine the Θ_{Bn} values, we first trace back the flow lines from a given virtual spacecraft inside the magnetosheath to the bow shock. The shock's surface is identified as an

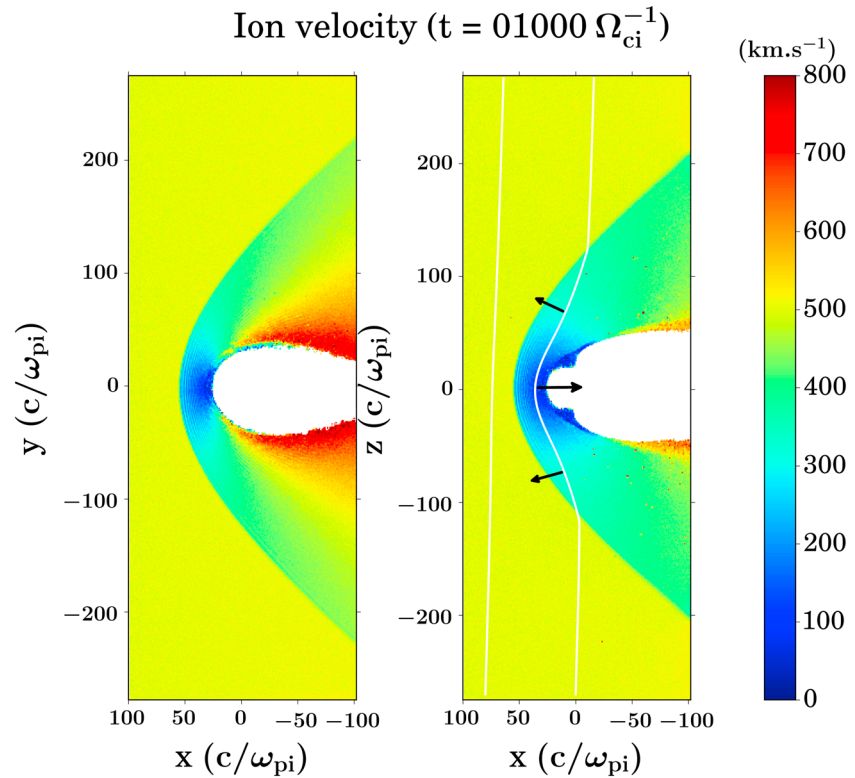


Figure 2. Total ion velocity in two 2-D cuts of the simulation domain, (left) in the equatorial plane and (right) in the noon-midnight meridian plane, at the end of the run ($t = 1000 \Omega_{ci}^{-1}$). The white curves in the Figure 2 (right) show two example magnetic field lines. The black arrows illustrate the orientation of the magnetic tension force inside the magnetosheath. Note that the magnetosphere, defined as the region where $n < 1.5 \text{ cm}^{-3}$, has been cut out in this figure.

isovalue surface of the magnetic field, and we use the normal to this surface to calculate the obliquity angle. We find that Θ_{Bn} ranges between 60° and 90° ; that is, the shock is in a quasi-perpendicular configuration upstream of all three spacecraft. The angle ψ in Figure 1 (fifth panel) quantifies the variation of the magnetic field orientation of the solar wind to the magnetosheath. The values of ψ are quite low, in particular, in the subsolar region (red curve) where they remain below 5° , indicating that the magnetic structure of the MC is essentially unchanged. Upstream of this spacecraft, Θ_{Bn} stays close to 90° during the entire MC. Farther on the flanks (blue and green curves), ψ does not exceed 30° and decreases as Θ_{Bn} increases. This suggests that the alteration of the magnetic field orientation across the bow shock is closely related to the value of Θ_{Bn} encountered upon entering the magnetosheath.

Figure 1 (fourth and fifth panels) can be directly compared to the two bottom panels in the first half of Figure 6 in Turc *et al.* [2014a], since it corresponds to a similar MC configuration. Note that the simulation ends when the central axis of the flux rope reaches Earth, and not after the whole flux rope has passed, because only the sign of the B_y component differs from the first half to the second half of the event considered here. The only difference is the sign of the B_z component upstream of the bow shock which is positive in Simulation 1 in order to prevent possible reconnection processes in the subsolar region, as they are not described in the Turc *et al.* [2014a] model. We find a very good agreement between the two approaches. Moreover, the absence of significant alteration of the MC's magnetic structure downstream of the quasi-perpendicular bow shock and the anticorrelation between Θ_{Bn} and ψ is confirmed by spacecraft observations inside the Earth's magnetosheath [Turc *et al.*, 2014b].

3.2. Impact of the MC on the Magnetosheath

In addition to the impact of the bow shock's crossing on the MC's structure, the hybrid model also allows us to investigate the response of the planetary environment to the MC's passage. First, the decrease of the Alfvén Mach number, due to the increase of the magnetic field strength at the MC's arrival, causes a sunward motion of the bow shock, consistent with theoretical expectations and spacecraft observations [e.g., Spreiter *et al.*,

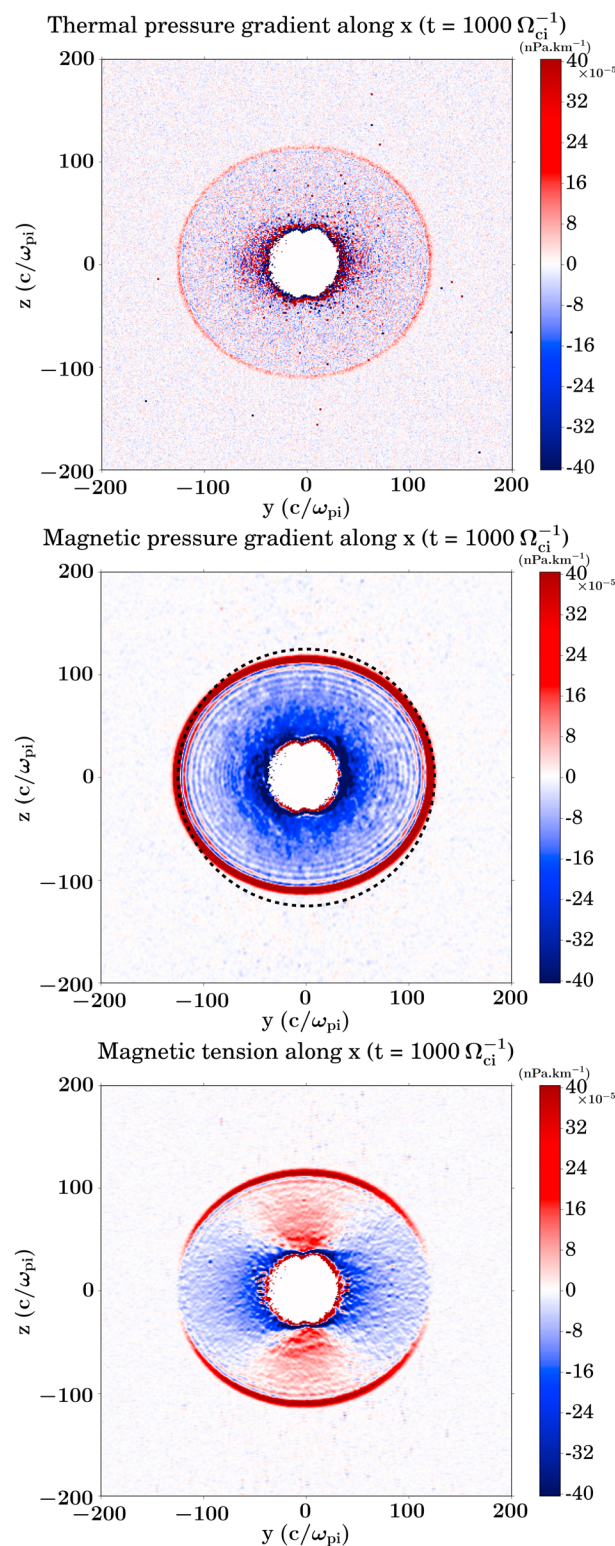


Figure 3. (top, middle, and bottom) Thermal pressure gradient along x , magnetic pressure gradient along x , and magnetic tension along x . The color maps are drawn in the terminator plane ($x = 0$) at the end of the run ($t = 1000 \Omega_{ci}^{-1}$). Note that the magnetosphere, defined as the region where $n < 1.5 \text{ cm}^{-3}$, has been cut out in this figure.

1966; Farris and Russell, 1994; Farrugia et al., 1995; Fairfield et al., 2001]. More interestingly, some of the global features of the magnetosheath seem to be closely related to the orientation of the magnetic field inside the MC. In particular, the ion velocity distribution in the magnetosheath strongly differs in the plane transverse to the upstream magnetic field lines and in the plane in which they lie. This is illustrated in Figure 2 which shows the total ion velocity in two two-dimensional cuts of the simulation domain at the end of the run ($t = 1000 \Omega_{ci}^{-1}$), i.e., when the magnetic field is directed along z . Note that the magnetosphere has been cut out to improve the clarity of the figure. In the noon-midnight meridian plane (Figure 2, right), we find a rather typical magnetosheath speed profile, with the flow reaccelerating progressively when moving tailward. This is, for example, comparable to that found in the work by Spreiter et al. [1966]. In a large part of the equatorial magnetosheath (Figure 2, left), however, the ion velocity along the flanks of the magnetopause exceeds by up to 1.6 times the upstream solar wind speed. Moreover, the position of this region of enhanced velocity rotates as the MC's passes by, that is, as the magnetic field turns from the y to the z direction, so that it remains in the plane perpendicular to the upstream magnetic field lines (not shown).

We examine the relative contributions of the different forces at play inside the magnetosheath, namely, the magnetic tension, the magnetic pressure gradient, and the thermal pressure gradient. We focus here on their x component, as the flow is essentially along this direction, in the terminator plane ($x = 0$), at the end of the run ($t = 1000 \Omega_{ci}^{-1}$). The investigation of the thermal pressure gradient along x (Figure 3, top) reveals that its contribution is globally lower than that of the other forces in the magnetosheath. Moreover, its distribution in the magnetosheath, as well as that of the magnetic pressure gradient (Figure 3, middle), is symmetric around the x axis and does not evolve with time (not shown). The near-circular rings displayed by the magnetic pressure

gradient inside the magnetosheath are signatures of the overshoot of the bow shock. Downstream of the shock, the magnetic field oscillates with a wavelength of the order of one ion gyroradius, and the magnetic pressure gradient reflects these oscillations. As the ion trajectories are calculated based on the weighted average of the magnetic field at the neighboring grid points, the ion gyromotion is resolved in the simulation even though the ion gyroradius is smaller than the cell size.

The magnetic tension, however, is not symmetrically distributed about the x axis inside the magnetosheath. This can be seen in Figure 3 (bottom) which shows the x component of the magnetic tension T_x . In the equatorial region, T_x is negative (in blue), indicating that it contributes to accelerate the particles towards the $-x$ direction, i.e., along the flow direction. On the contrary, at higher latitudes, T_x is positive (in red) and thus tends to slow down the plasma flow. As the enhanced flows, the regions of positive/negative T_x rotate as the MC's passes by: at the MC's arrival, when the magnetic field is parallel to the y axis, T_x accelerates the polar flows and decelerates the equatorial flows (not shown). The opposite signs of the T_x component in the plane perpendicular to the interplanetary magnetic field (IMF) and in the plane in which it lies are consistent with the deformation of the field lines around the magnetosphere. At $t = 1000 \Omega_{ci}^{-1}$, the magnetic field is pointing northward and the field lines mostly bend in the noon-midnight meridian plane. This is illustrated in Figure 2 where two example field lines are drawn in white. The black arrows perpendicular to the draped field line in the magnetosheath illustrate the direction of the magnetic tension force.

As the draped flux tubes slide around the magnetopause, the accumulated magnetic tension is released and accelerate the particles in a so-called magnetic slingshot effect. The enhanced flows in the equatorial plane are thus due to the cumulative effects of the magnetic tension and the magnetic pressure gradient. On the contrary, in the noon-midnight meridian plane, only the latter acts to accelerate the flow, whereas the magnetic tension tends to decelerate it. The magnetic tension force is thus the cause of the asymmetric velocity distribution inside the magnetosheath (see Figure 2).

Spacecraft observations in the Earth's magnetosheath have provided evidence of such accelerated flows exceeding the solar wind speed near the flank magnetopause [e.g., *Chen et al.*, 1993; *Rosenqvist et al.*, 2007; *Lavraud et al.*, 2007, 2013; *Harris et al.*, 2013, and references therein]. In particular, *Lavraud et al.* [2013] highlight that the position of the region of enhanced velocities is related to the orientation of the upstream magnetic field. *Chen et al.* [1993] first attribute these flows to the magnetic tension released from the draped field lines. More recently, using global MHD simulations, *Lavraud et al.* [2007] find that in the region of enhanced speeds, the contribution of the magnetic tension and of the magnetic pressure gradient to accelerating the flows are comparable, whereas that of the thermal pressure gradient is negligible. This suggests that these enhanced flows arise when the magnetic forces play a predominant role in the dynamics of the magnetosheath, i.e., when the plasma β is low [*Lavraud et al.*, 2007, 2013]. Consequently, this phenomenon is generally observed during interplanetary coronal mass ejections because of the long intervals of low plasma β associated to these solar wind transients. Our results with a hybrid simulation are consistent with those previous studies but also complement them by showing that in the plane containing the IMF, only the magnetic pressure gradient accelerates the flow, while the magnetic tension, directed in the opposite direction, slows it down.

3.3. Impact of the MC on the Boundaries

As a consequence of these enhanced flows, the magnetopause is compressed in the plane perpendicular to the IMF. This compression is caused by the higher dynamic pressure in this region, due to the increased velocities. This can be seen in Figure 2, where the white area corresponds to the magnetosphere and shows that the flaring of the tail is much larger in the noon-midnight meridian plane (Figure 2, right) than in the equatorial plane (Figure 2, left). The magnetopause cross section in a plane transverse to the x axis is elliptical, and its major axis is parallel to the interplanetary magnetic field lines. This is consistent with the findings of *Lavraud et al.* [2013].

The bow shock cross section is also elliptical, but the oval is this time elongated perpendicularly to the IMF. For example, at the end of the simulation, the bow shock shape is slightly oblate because of the due north magnetic field. This is illustrated for instance in Figure 3 (middle), where the bow shock can be identified as the red boundary between the solar wind (in white) and the magnetosheath (in blue). The deviation from a circular shape, relatively small in the terminator plane, is highlighted by the dashed black circle, of radius $125 c/\omega_{pi}$. The direction of the elongation of the bow shock cross section rotates with the upstream magnetic field and remains perpendicular to its direction (not shown). Very recently, *Sibeck and Lin* [2014] have reported a similar deformation of the bow shock in the plane transverse to the Sun-Earth line in MHD

simulations of the geomagnetic tail. They argue that this elliptical shape is due to higher fast-mode speeds in the direction perpendicular to the magnetic field lines and that the deformation of the bow shock becomes more pronounced and is detectable closer to Earth as the magnitude of the magnetic field increases.

In conclusion, Simulation 1 shows that the hybrid model reproduces satisfactorily the interaction of an MC with the Earth's environment and the alteration of its magnetic structure in the magnetosheath, as well as the response of the planetary environment to the varying magnetic field associated to the MC. In particular, it describes the enhanced flows arising in the regions of the magnetosheath perpendicular to the upstream magnetic field lines, which have been observed in the Earth's magnetosheath and in MHD simulations. This asymmetric velocity distribution inside the magnetosheath is attributed to the magnetic tension force which accelerates the particles perpendicularly to the magnetic field lines. The hybrid simulation also predicts that this force acts to decelerate the flow in the plane in which the flux tubes lie. Finally, the cross sections of the magnetopause and the bow shock in the terminator plane are both elliptical but are elongated in different directions, along and transverse to the magnetic field lines, respectively.

4. Simulation 2: Magnetic Cloud With a Large B_x Component

In Simulation 2, we now set the orientation of the MC's magnetic field so that a large part of the bow shock is in quasi-parallel configuration. In the initialization phase, the cone angle is equal to 20° , that is, the magnetic field has a large B_x component.

4.1. Validation of the Foreshock Description

The only difference with the initial stage of Simulation 1 is the direction of the upstream magnetic field, but this change has major consequences on the bow shock properties. Because of the quasi-radial magnetic field in Simulation 2 (i.e., the magnetic field is roughly aligned with the solar wind flow), the quasi-parallel region of the bow shock lies rather close to the subsolar point and covers a large part of the dayside bow shock. Upstream of the quasi-parallel shock, the backstreaming particles form the foreshock and their interaction with the incoming solar wind gives rise to waves and instabilities. Therefore, contrary to Simulation 1 where the ion dynamics played little role in the large-scale phenomena we discussed in section 3, it is necessary to include ion kinetic effects in Simulation 2 in order to self-consistently simulate the ion foreshock.

Shown in Figure 4 (top row) are the magnetic field strength, the ion density, and temperature in the equatorial plane of the simulation domain before the MC's arrival. Consistent with the orientation of the upstream magnetic field, indicated by a white arrow in Figure 4 (top left), the quasi-parallel bow shock and its associated foreshock are located on the duskside of the equatorial plane. The foreshock appears as an extended region of highly-fluctuating magnetic field, density, and temperature, as can be seen in the upper half of the three color maps in Figure 4. We note in particular that the temperature is higher in the foreshock than in the unperturbed solar wind. This temperature enhancement is due to the energetic backstreaming population [Omid *et al.*, 2005; Blanco-Cano *et al.*, 2006].

Figure 4 (top row) shows the presence of field-aligned cavities in the foreshock, where the magnetic field and the density are lower and the temperature higher than in the pristine solar wind. These cavities are separated by denser filaments, where the magnetic field is enhanced and the temperature is low. Similar field-aligned cavities are reported in the 3-D hybrid simulations carried out by Lin and Wang [2005]. The transverse wavelength of these structures is of the order of $25 c/\omega_{pi}$ in our simulation, consistent with that obtained by Lin and Wang [2005].

We now examine in more detail the wave properties in the foreshock along the two trajectories drawn in white in Figure 4 (top left). Cut 1 is parallel to the IMF and the magnetic field components and strength, as well as the ion density, along this trajectory are displayed in Figure 4 (bottom left). The magnetic field components (Figures 4a–4c, trajectory 1) reveal the presence of sinusoidal waves. In the left-hand half of the plot, the magnetic field strength (Figure 4d, trajectory 1) and the ion density (Figure 4e, trajectory 1) show very little variation, denoting that these waves are only weakly compressional. When moving closer to the shock, i.e., towards the right side of the plot, the amplitude of the sinusoidal waves increases, and fluctuations of the magnetic field magnitude and of the ion density arise. Deep in the foreshock, compressive waves transverse to the IMF are also observed, as evidenced by the parameters plotted in Figure 4 (bottom right), which are taken along trajectory 2. There, the variations of the magnetic field direction are accompanied by correlated fluctuations of the magnetic field magnitude and the ion density.

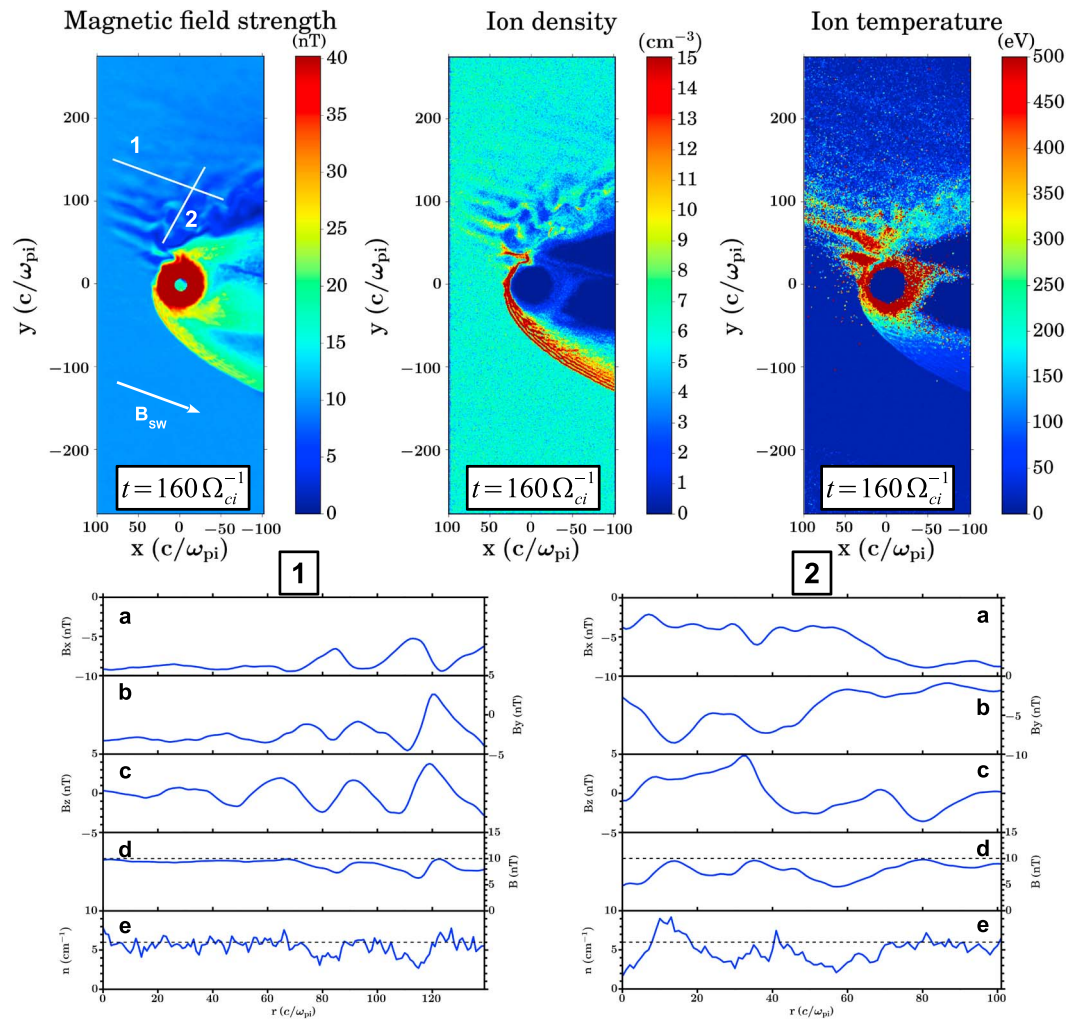


Figure 4. (top row) Magnetic field strength, ion density, and temperature in the equatorial plane before the MC's arrival ($t = 160 \Omega_{ci}^{-1}$). (bottom row) Magnetic field and density along trajectories (left) 1 and (right) 2 in the foreshock, parallel and perpendicular to the field lines, respectively. The position of trajectories 1 and 2 in the simulation domain is displayed in Figure 4 (top left). The parameter r on the abscissa of the lines plots corresponds to the distance from the beginning of the cut. The dashed lines in the magnetic field magnitude and density panels indicate the values of these parameters in the unperturbed solar wind.

These results concerning the different wave properties in the foreshock are in good agreement with those obtained by *Blanco-Cano et al.* [2006] with a simulated magnetosphere 10 times smaller than Earth's. Note that in their work, the sinusoidal waves along the magnetic field lines are only weakly compressional because the analyzed trajectory starts farther away from the shock. Also, the decrease of the amplitude of the density and magnetic field strength fluctuations when moving away from the shock is consistent with the findings of *Wang et al.* [2009] using 3-D hybrid-particle-in-cell simulations and of *von Althaus et al.* [2014] using hybrid Vlasov simulations. Spacecraft observations in the terrestrial foreshock have shown evidence of similar sinusoidal waves accompanied by density variations [e.g., *Eastwood et al.*, 2005]. The presence of compressional waves in the foreshock indicates that we have a fully developed quasi-parallel shock, as is the case for the Earth's bow shock [*Omidi et al.*, 2005; *Blanco-Cano et al.*, 2006].

4.2. Simulation Results

We now move on to the subsequent times of Simulation 2, when the MC interacts with the planetary environment. As B_x is kept constant, the enhancement of the B_y component in Step 2 (see section 2) causes this time a rotation of the magnetic field direction, and the cone angle increases to 47° when the magnetic field strength is maximum. In this simulation, the magnetic field magnitude inside the MC is equal to 13.9nT. The associated M_A is 4, and the upstream plasma β is equal to 0.17. At the beginning of Step 3, the upstream magnetic field

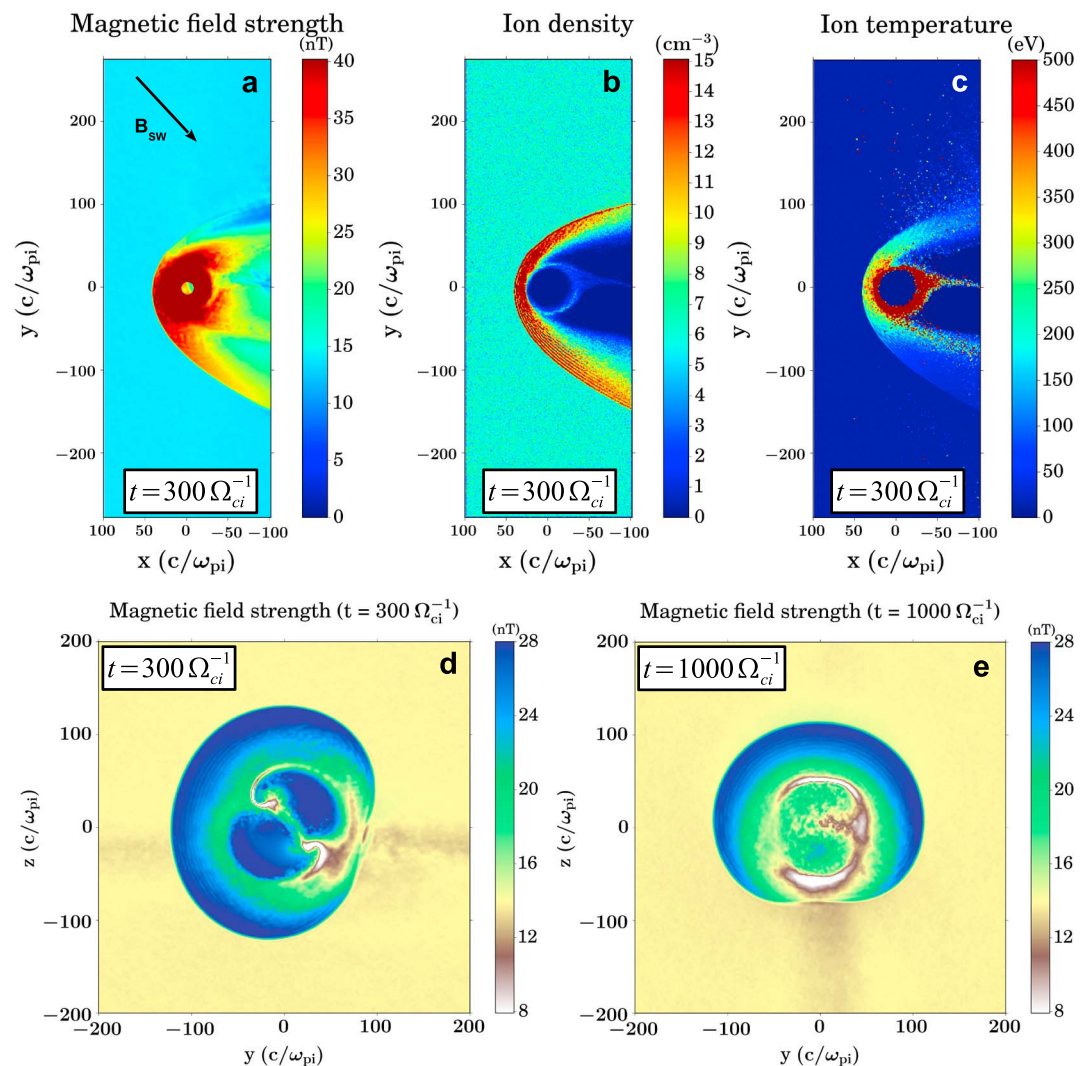


Figure 5. (top row) Magnetic field strength, ion density, and temperature in the equatorial plane at the beginning of the rotation of the MC's magnetic field ($t = 300 \Omega_{ci}^{-1}$). (bottom row) Magnetic field strength in a 2-D cut of the simulation domain at $x = -50 c/\omega_{pi}$, (top) at the beginning ($t = 300 \Omega_{ci}^{-1}$) and (bottom) at the end ($t = 1000 \Omega_{ci}^{-1}$) of the rotation of the MC's magnetic field.

displays an ortho-Parker spiral-like orientation and then progressively turns from the equatorial plane to the noon-midnight meridian plane while the cone angle remains constant.

Figures 5a–5c show the same parameters as Figure 4 (top row), that is, the magnetic field strength, the ion density, and temperature, in the equatorial plane, but at $t = 300 \Omega_{ci}^{-1}$, i.e., after the magnetic field magnitude has increased. Note that the scales used are the same as in Figure 4. According to the orientation of the upstream magnetic field, the quasi-parallel region should still be located on the dusk flank of the bow shock, though a bit farther from the subsolar point because of the increase of the IMF cone angle (see black arrow in Figure 5a). However, neither the magnetic field strength nor the ion density shows any evidence of the existence of the ion foreshock. Only the ion temperature (Figure 5c) gives a hint of the presence of the backstreaming particles upstream of the dusk flank bow shock. The foreshock therefore still exists after the MC's arrival but is much fainter than at the beginning of the simulation.

The MC's arrival results in both a variation of the magnetic field direction and an increase of its intensity. The attenuation of the foreshock in our simulation is most likely caused by the enhancement of the magnetic field strength or more precisely by the ensuing decrease of the Alfvén and magnetosonic Mach numbers. If the upstream Mach number is lower, then less energy dissipation is required for the flow to become

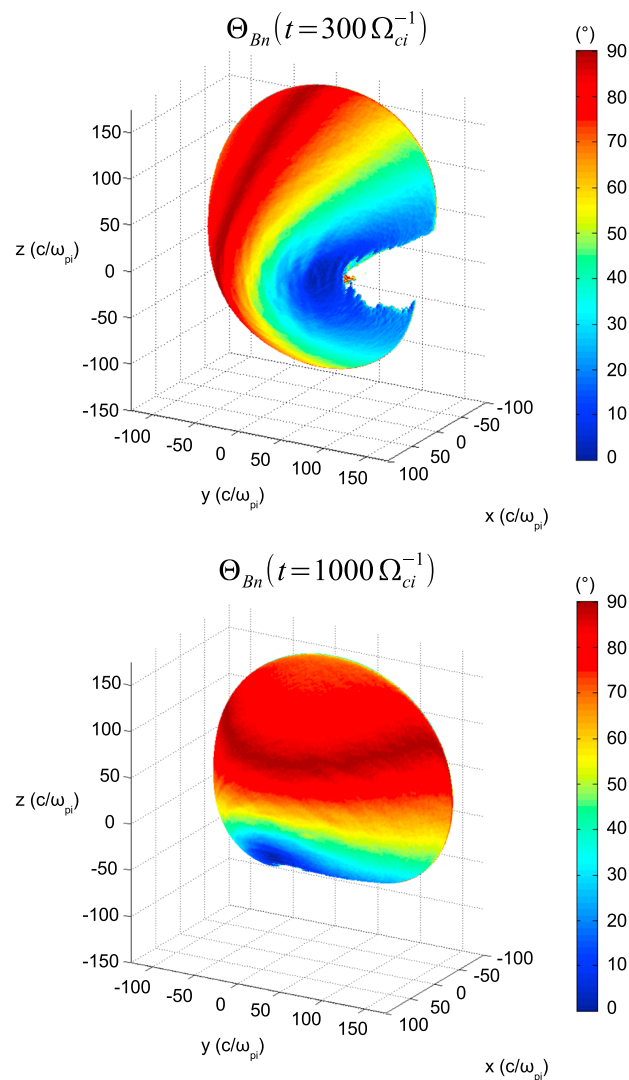


Figure 6. Color-coded values of the Θ_{Bn} angle, mapped onto the bow shock's surface (top) at the beginning ($t = 300 \Omega_{ci}^{-1}$) and (bottom) at the end ($t = 1000 \Omega_{ci}^{-1}$) of the rotation of the MC's magnetic field. See text for more detail.

shape of the bow shock is not symmetric about the x axis but that its duskside lies closer to the magnetosphere as if pushed inward. Also, the intensity of the magnetic field downstream of the bow shock is much lower in the duskside than in the rest of the magnetosheath. These two features are signatures of the quasi-parallel bow shock configuration. The fact that the quasi-parallel shock lies closer to the magnetosphere than the quasi-perpendicular was previously reported, for example, by *Lin et al.* [1996] in 2-D simulations. In the present work, the inclusion of the third dimension reveals that the cross section of the bow shock in the plane tangential to the Sun-Earth line departs from an ellipsoid. Its quasi-parallel region appears as a depression, most clearly seen in Figure 5e in the southern part of the bow shock. This indentation in the bow shock shape is the consequence of the energy loss due to the particles reflected on the shock's surface.

Figures 5a and 5d reveal that the intensity of the magnetic field further decreases when moving deeper in the quasi-parallel magnetosheath, reaching values much lower than in the solar wind. Such behavior may stem from the fact that the magnetospheric and magnetosheath field lines are close to being antiparallel in this region, according to the orientation of the magnetic field on both sides of the magnetopause. Therefore, the decrease of the total magnetic field strength may derive from the sum of these two oppositely oriented magnetic fields which diminishes the more antiparallel the field lines become. Similarly low magnetic field

submagnetosonic. Therefore, the number of particles reflected at the bow shock's surface is expected to decrease together with the M_A , hence the weakening of the foreshock during the MC.

On the other hand, the variation of the upstream magnetic field orientation causes the foreshock to move farther from the subsolar region but should not affect to a great extent its overall properties. This is supported by studies of the interaction of rotational discontinuities with the Earth's bow shock, which show that the quasi-parallel region and its associated foreshock reform in another part of the bow shock after a change of the IMF direction [*Lin et al., 1996; Karimabadi et al., 2014*] but do not suggest any strong modification of their global features.

To test this hypothesis, we have performed another simulation with the same MC configuration but a larger M_A . In this additional simulation, the M_A inside the MC is equal to the M_A at the beginning of Simulation 2. We find that when $M_A = 5.6$ during the MC, the foreshock remains as strong as at $t = 160 \Omega_{ci}^{-1}$ in Simulation 2 (not shown). This confirms that the strength of the foreshock is linked to the upstream M_A and not to the magnetic field direction.

Shown in Figure 5d is the magnetic field strength in the plane at $x = -50 c/\omega_{pi}$ of the simulation domain, again at $t = 300 \Omega_{ci}^{-1}$. Note that the color scale is different from that used in Figure 5a to accommodate the faint foreshock, which is visible in brown. First, we find that the

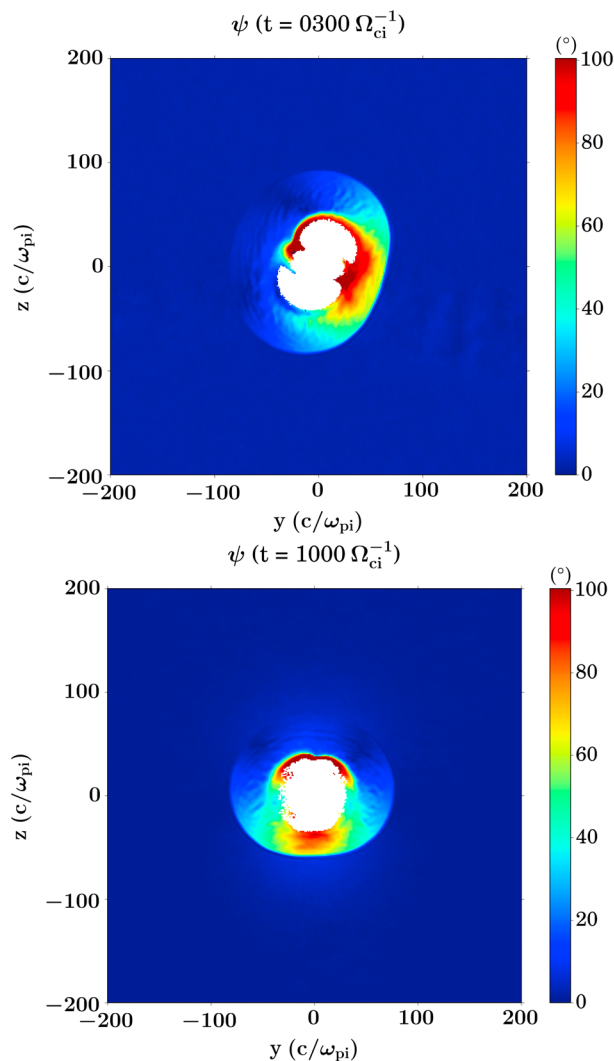


Figure 7. Color-coded values of the angle ψ in the terminator plane ($x = 0$), (top) at the beginning ($t = 300 \Omega_{ci}^{-1}$) and (bottom) at the end ($t = 1000 \Omega_{ci}^{-1}$) of the rotation of the MC's magnetic field. ψ is defined as the angle between the magnetic field at a given location and that at the entry of the simulation domain. Note that the magnetosphere, defined as the region where $n < 1.5 \text{ cm}^{-3}$, has been cut out in this figure.

In order to investigate the alteration of the MC's structure across the bow shock, we calculate the angle ψ between the magnetic field in the magnetosheath and that in the unperturbed solar wind, which quantifies the variation of the magnetic field direction. Figure 7 shows its values in the terminator plane at $t = 300 \Omega_{ci}^{-1}$ (top) and at $t = 1000 \Omega_{ci}^{-1}$ (bottom). In Figures 7 (top) and 7 (bottom), ψ is highest downstream of the quasi-parallel bow shock and exceeds 80° in a significant part of the magnetosheath. In addition, large magnetic field fluctuations arise (not shown). Therefore, the MC's magnetic structure is strongly modified when it encounters a shock in quasi-parallel configuration. On the contrary, it remains roughly unchanged downstream of the quasi-perpendicular shock, as shown by the low ψ values, mostly below 20° , in the left-hand (upper) part of the top (bottom) panel of Figure 7. Since these two regimes, quasi-parallel and quasi-perpendicular, are present simultaneously in different parts of the bow shock, the MC's structure differs from one region of the magnetosheath to another. Also, as Θ_{Bn} changes with the upstream magnetic field orientation, the alteration of the MC's structure in a given part of the magnetosheath varies with time.

intensities in the quasi-parallel magnetosheath are obtained, for example, by *Omidi et al.* [2014] using 2.5-D global hybrid simulations.

As the MC's magnetic field rotates, the signatures of the quasi-parallel regime move along the bow shock surface and are observed in the southern bow shock at $t = 1000 \Omega_{ci}^{-1}$ (see Figure 5e). In particular, Figures 5d and e show evidence of the rotation of the foreshock from the dusk-side of the equatorial plane to the south part of the noon-midnight meridian plane as the MC passes by.

Figure 6 (top) displays the values of Θ_{Bn} at $t = 300 \Omega_{ci}^{-1}$ mapped onto the bow shock surface, identified as an isovalue surface of the magnetic field strength. Part of the bow shock is missing in the right-hand side of the figure, since the magnetic field fluctuates largely in this region and no continuous isovalue surface can be identified. The values of the shock obliquity indicate that the duskside bow shock is in a quasi-parallel configuration, with Θ_{Bn} being particularly low, around 10° , near the equatorial plane. Θ_{Bn} then increases when moving towards higher latitudes, and the entire dawnside hemisphere as well as the polar regions are located downstream of a quasi-perpendicular bow shock. As was expected from the position of the foreshock at $t = 1000 \Omega_{ci}^{-1}$ (Figure 5e), the quasi-parallel region has moved from the duskside to the southern part of the bow shock at the end of the simulation (Figure 6, bottom), following the rotation of the MC's magnetic field. The large-scale structuring of the bow shock is thus controlled by the MC's varying magnetic field.

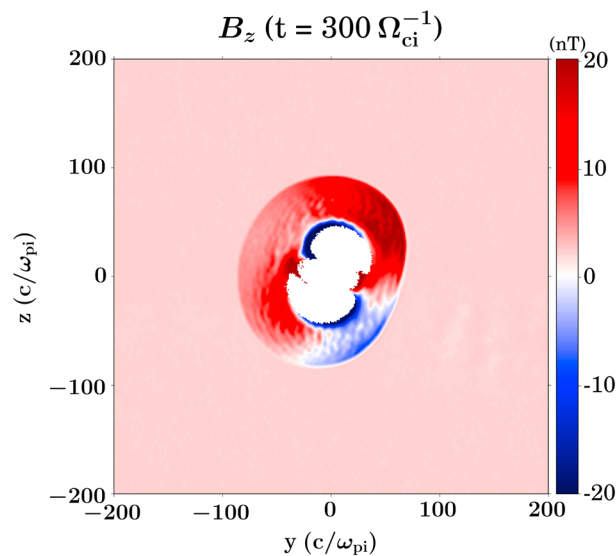


Figure 8. Color map of the B_z component of the magnetic field in the terminator plane ($x = 0$) at the beginning of the rotation of the MC's magnetic field ($t = 300 \Omega_{ci}^{-1}$). Note that the magnetosphere, defined as the region where $n < 1.5 \text{ cm}^{-3}$, has been cut out in this figure.

Finally, we examine the variation of the B_z component inside the magnetosheath because of its important role in reconnection processes between the solar wind and the Earth's magnetic fields. When estimating an MC's impact in the magnetosphere, it is generally assumed that its magnetic field direction does not change from the upstream solar wind to the magnetopause. However, we have shown that it can significantly vary when crossing a shock in quasi-parallel configuration. This large variation can lead to a reversal of the B_z component in a part of the magnetosheath, as illustrated in Figure 8 which displays the value of B_z in the terminator plane at $t = 300 \Omega_{ci}^{-1}$. Although B_z is positive (in red) in the incoming solar wind and in the major part of the magnetosheath, a region of negative B_z (in blue) emerges in the duskside of the southern magnetosheath, downstream of the

quasi-parallel bow shock. A northward B_z can thus turn south, and conversely, when traversing from the solar wind to some parts of the magnetosheath. This confirms the results obtained by *Turc et al.* [2014a] with a semianalytical magnetosheath model. The modification of the sign of B_z will most likely have a strong impact on the reconnection pattern at the magnetopause, but this lies beyond the scope of this paper.

5. Discussion and Conclusions

In this paper, we have presented the first 3-D global hybrid simulations of the interaction of an MC with a planetary bow shock. Hybrid simulations provide us with a self-consistent description of the response of the planetary environment to the MC's time-varying parameters. They also offer the opportunity to explore the quasi-parallel region of the bow shock, and its associated foreshock since the ion dynamics is taken into account. We focus here on the inner part of the MCs, where their magnetic field rotates smoothly. The MCs are thus modeled by an increase of the magnetic field magnitude followed by a slow rotation of their direction. The results of two runs, corresponding to two different MC orientations, are described. In both cases, we examine how the MC's structure is altered when crossing the bow shock, and how its passage affects in turn the outer parts of the planetary environment, from the foreshock to the magnetopause. The following conclusions were reached:

1. At the MC's arrival, we find that the decrease of the Alfvén Mach number due to the enhanced magnetic field strength causes an attenuation of the foreshock region. We interpret this as a consequence of the lesser energy dissipation required at the bow shock if the upstream Mach number is lower.
2. Since the upstream magnetic field orientation directly controls the shock configuration, the values of the shock obliquity angle, Θ_{Bn} , vary as the MC passes by. This is particularly noticeable when Θ_{Bn} reaches low values as we show that the quasi-parallel region moves along the bow shock surface, accompanied by its associated ion foreshock.
3. Inside the magnetosheath, the magnetic forces are predominant because of the low plasma β and give rise to asymmetric flows. We ascribe them to the magnetic tension which acts in opposite directions in the plane perpendicular to the upstream magnetic field lines and in the plane in which they lie. Also, the position of the regions of positive/negative magnetic tension follows the rotation of the MC's magnetic field and so do the asymmetric flows. We predict that the magnetic tension tends to slow down the flow in the plane containing the magnetic field lines.
4. The cross sections of the magnetopause and the bow shock in the plane transverse to the x axis are both elliptical, but the orientation of their major axis is perpendicular to one another. The deformation of the

magnetopause is attributed to the higher dynamic pressure in the regions of enhanced flows and that of the bow shock to different fast-mode speeds perpendicular and parallel to the magnetic field lines [Sibeck and Lin, 2014]. We also find that the quasi-parallel region of the bow shock is another source of asymmetry in the shape of this boundary, as it creates an indentation in the bow shock surface. This dent is most likely caused by the energy loss due to the particles reflected on the shock's surface.

5. The alteration of the magnetic structure of MCs across the bow shock is closely related to the encountered shock obliquity: the variation of their magnetic field orientation increases as Θ_{bn} decreases. If Θ_{bn} is close to 90° , the MC's smooth rotation is virtually unchanged downstream of the bow shock, as expected from Rankine-Hugoniot equations. When the shock is in a quasi-parallel geometry ($\Theta_{bn} \leq 45^\circ$), the modification of the MC's magnetic structure becomes significant, and the orientation of the MC's magnetic field can vary by more than 80° . In addition, large magnetic field fluctuations are observed in the quasi-parallel magnetosheath, which alter even more the MC's smoothly rotating magnetic field. The numerical simulations provide quantitative estimates of the modification of an MC's structure downstream of the bow shock.
6. We find that B_z can reverse in a sizable part of the region downstream of the quasi-parallel shock and thus that a southward B_z and a northward B_z can simultaneously be observed inside the magnetosheath. The possible reversal of B_z downstream of the bow shock was predicted by the Turc *et al.* [2014a] magnetosheath model and is now further supported by our hybrid simulations.

Our results show that the alteration of the magnetic structure of MCs from the solar wind to the magnetosheath changes drastically depending on the encountered shock geometry. The different impacts of the quasi-parallel and quasi-perpendicular shocks on the MC's magnetic field can be attributed to the radically different properties of these two regimes. First, in the quasi-parallel domain, the MC first interacts with the foreshock. The waves and the transient structures that develop in this region most likely alter the MC's magnetic structure. Second, the extent of the quasi-parallel shock transition is much larger than that of the quasi-perpendicular shock. The coupling between the fields and the particles may be stronger since they have more time to interact while crossing the shock. The impact of the ions on the magnetic field may be more important and cause a rotation of its direction. Third, the level of fluctuations is much higher in the quasi-parallel region, and the shock is nonstationary. This again can contribute to modifying the MC's magnetic field. The significant alteration of the MC across the quasi-parallel bow shock most likely results from a combination of these effects.

Reconnection processes at the magnetopause were not examined in the present paper but are expected to take place tailward of the cusps in the simulations discussed here because of the northward orientation of the MC's magnetic field. However, this estimation of the regions of reconnection is based only on the magnetic field direction upstream of the bow shock. Yet in Simulation 2 the coexistence of positive and negative B_z inside the magnetosheath suggests that unusual reconnection patterns may arise. In particular, the southward turning of an initially northward magnetic field could give rise to a region of antiparallel magnetic fields near the equatorial plane [see Turc *et al.*, 2014a], which could more efficiently drive magnetospheric disturbances than expected for positive B_z . Thus, the interaction of an MC with the bow shock and its propagation into the magnetosheath could possibly modify that MC's geoeffectivity. In this case, the role played by the magnetosheath should be taken into account to refine the prediction of that MC's impact on the Earth's environment.

Another important feature of the interaction of MCs with the terrestrial magnetosheath is the emergence of fast asymmetric flows near the magnetopause which can significantly alter the solar wind/magnetosphere coupling through surface waves and the Kelvin-Helmholtz instability (KHI) [Chen *et al.*, 1993; Rosenqvist *et al.*, 2007; Fairfield *et al.*, 2007; Lavraud and Borovsky, 2008]. The enhanced flows increase the velocity shear between the magnetospheric and magnetosheath plasmas, which controls the development of the KHI [Walker, 1981]. Lavraud and Borovsky [2008] suggest that a lower Alfvén Mach number should lead to a faster wave growth rate. Further investigation of this effect is left for future work.

The attenuation of the foreshock at the MC's arrival, attributed to the decrease of the M_A , could also have important implications in the solar wind/magnetosphere coupling during MCs. The damping of the foreshock turbulence could result in a level of fluctuations lower than usual in the quasi-parallel magnetosheath. This could possibly affect reconnection processes, as well as KHI at the magnetopause. The evolution of the foreshock properties during MCs and their impact on the solar wind/magnetosphere coupling should be investigated in the future. However, because of the rather low N_{ppc} , the attenuation of the foreshock at the

MC's arrival may be overestimated in our simulation, as the number of shock-reflected particles decreases. If closer investigation of this process is to be undertaken, it will be necessary to increase the N_{ppc} to improve the statistics of counterstreaming particles in the foreshock.

In this study, we have mostly focused on the large-scale MC/bow shock interaction. However, hybrid simulations also offer the opportunity to investigate phenomena taking place at the ion scales. The influence of the foreshock region on the MC's magnetic structure and conversely the impact of the MC on the foreshock, but also how the turbulence evolves inside the magnetosheath as the MC passes by, will be examined in more detail in the future. With a longer-term outlook, including the interplanetary shock, which often precedes MCs, and the turbulent sheath it generates would take the simulations of the MC/bow shock interaction one step further.

To conclude, the results of the present study show that the bow shock and the magnetosheath play an important role in the interaction of MCs with the Earth's environment. They can significantly alter an MC's magnetic structure, but their properties are also simultaneously strongly modified by the MC. This results in an unusual solar wind/magnetosphere coupling, which is still poorly known. Further investigation is therefore required to attain a better understanding of how MCs interact with the terrestrial magnetosphere.

Acknowledgments

This work has been done within the LABEX Plas@par project and received financial state aid managed by the Agence Nationale de la Recherche, as part of the programme "Investissements d'avenir" under the reference ANR-11-IDEX-0004-02. Alexis Jeandet and Bruno Katra are thanked for technical support. L.T. is supported by an ESA Research Fellowship in Space Science. The data used to produce the figures in the paper are available from the authors upon request.

Yuming Wang thanks two anonymous reviewers for their assistance in evaluating this paper.

References

- Birdsall, C. K., and A. B. Langdon (1985), *Plasma Physics Via Computer Simulation*, McGraw-Hill, New York.
- Blanco-Cano, X., N. Omid, and C. T. Russell (2006), Macrostructure of collisionless bow shocks: 2. ULF waves in the foreshock and magnetosheath, *J. Geophys. Res.*, *111*, A10205, doi:10.1029/2005JA011421.
- Burlaga, L. F. (1988), Magnetic clouds and force-free fields with constant alpha, *J. Geophys. Res.*, *93*, 7217–7224, doi:10.1029/JA093iA07p07217.
- Burlaga, L. F., E. Sittler, F. Mariani, and R. Schwenn (1981), Magnetic loop behind an interplanetary shock—Voyager, Helios, and IMP 8 observations, *J. Geophys. Res.*, *86*, 6673–6684, doi:10.1029/JA086iA08p06673.
- Chen, S.-H., M. G. Kivelson, J. T. Gosling, R. J. Walker, and A. J. Lazarus (1993), Anomalous aspects of magnetosheath flow and of the shape and oscillations of the magnetopause during an interval of strongly northward interplanetary magnetic field, *J. Geophys. Res.*, *98*, 5727–5742, doi:10.1029/92JA02263.
- Eastwood, J. P., E. A. Lucek, C. Mazelle, K. Meziane, Y. Narita, J. Pickett, and R. A. Treumann (2005), The foreshock, *Space Sci. Rev.*, *118*, 41–94, doi:10.1007/s11214-005-3824-3.
- Echer, E., M. V. Alves, and W. D. Gonzalez (2005), A statistical study of magnetic cloud parameters and geoeffectiveness, *J. Atmos. Sol. Terr. Phys.*, *67*, 839–852, doi:10.1016/j.jastp.2005.02.010.
- Echer, E., W. D. Gonzalez, and B. T. Tsurutani (2008a), Interplanetary conditions leading to superintense geomagnetic storms ($Dst \leq -250$ nT) during solar cycle 23, *Geophys. Res. Lett.*, *35*, L06S03, doi:10.1029/2007GL031755.
- Echer, E., W. D. Gonzalez, B. T. Tsurutani, and A. L. C. Gonzalez (2008b), Interplanetary conditions causing intense geomagnetic storms ($Dst \leq -100$ nT) during solar cycle 23 (1996–2006), *J. Geophys. Res.*, *113*, A05221, doi:10.1029/2007JA012744.
- Erkaev, N. V., C. J. Farrugia, B. Harris, and H. K. Biernat (2011), On accelerated magnetosheath flows under northward IMF, *Geophys. Res. Lett.*, *38*, L01104, doi:10.1029/2010GL045998.
- Erkaev, N. V., C. J. Farrugia, A. V. Mezentssev, R. B. Torbert, and H. K. Biernat (2012), Accelerated magnetosheath flows caused by IMF draping: Dependence on latitude, *Geophys. Res. Lett.*, *39*, L01103, doi:10.1029/2011GL050209.
- Fairfield, D. H., I. H. Cairns, M. D. Desch, A. Szabo, A. J. Lazarus, and M. R. Aellig (2001), The location of low Mach number bow shocks at Earth, *J. Geophys. Res.*, *106*, 25,361–25,376, doi:10.1029/2000JA000252.
- Fairfield, D. H., M. M. Kuznetsova, T. Mukai, T. Nagai, T. I. Gombosi, and A. J. Ridley (2007), Waves on the dusk flank boundary layer during very northward interplanetary magnetic field conditions: Observations and simulation, *J. Geophys. Res.*, *112*, A08206, doi:10.1029/2006JA012052.
- Farris, M. H., and C. T. Russell (1994), Determining the standoff distance of the bow shock: Mach number dependence and use of models, *J. Geophys. Res.*, *99*, 17,681–17,689, doi:10.1029/94JA01020.
- Farrugia, C. J., N. V. Erkaev, H. K. Biernat, and L. F. Burlaga (1995), Anomalous magnetosheath properties during Earth passage of an interplanetary magnetic cloud, *J. Geophys. Res.*, *100*, 19,245–19,258, doi:10.1029/95JA01080.
- Farrugia, C. J., N. V. Erkaev, V. K. Jordanova, N. Lugaz, P. E. Sandholt, S. Mühlbacher, and R. B. Torbert (2013), Features of the interaction of interplanetary coronal mass ejections/magnetic clouds with the Earth's magnetosphere, *J. Atmos. Sol. Terr. Phys.*, *99*, 14–26, doi:10.1016/j.jastp.2012.11.014.
- Goodrich, C. C., J. G. Lyon, M. Wiltberger, R. E. Lopez, and K. Papadopoulos (1998), An overview of the impact of the January 10–11 1997 magnetic cloud on the magnetosphere via global MHD simulation, *Geophys. Res. Lett.*, *25*, 2537–2540, doi:10.1029/98GL01159.
- Gopalswamy, N., S. Akiyama, S. Yashiro, G. Michalek, and R. P. Lepping (2008), Solar sources and geospace consequences of interplanetary magnetic clouds observed during solar cycle 23, *J. Atmos. Sol. Terr. Phys.*, *70*, 245–253, doi:10.1016/j.jastp.2007.08.070.
- Harris, B., C. J. Farrugia, N. V. Erkaev, and R. B. Torbert (2013), Observational aspects of IMF draping-related magnetosheath accelerations for northward IMF, *Ann. Geophys.*, *31*, 1779–1789, doi:10.5194/angeo-31-1779-2013.
- Huttunen, K. E. J., and H. E. J. Koskinen (2004), Importance of post-shock streams and sheath region as drivers of intense magnetospheric storms and high-latitude activity, *Ann. Geophys.*, *22*, 1729–1738, doi:10.5194/angeo-22-1729-2004.
- Huttunen, K. E. J., H. E. J. Koskinen, and R. Schwenn (2002), Variability of magnetospheric storms driven by different solar wind perturbations, *J. Geophys. Res.*, *107*(A7), 1121, doi:10.1029/2001JA900171.
- Huttunen, K. E. J., R. Schwenn, V. Bothmer, and H. E. J. Koskinen (2005), Properties and geoeffectiveness of magnetic clouds in the rising, maximum and early declining phases of solar cycle 23, *Ann. Geophys.*, *23*(2), 625–641, doi:10.5194/angeo-23-625-2005.
- Jeřáb, M., Z. Němeček, J. Šafránková, K. Jelínek, and J. Měrka (2005), Improved bow shock model with dependence on the IMF strength, *Planet. Space Sci.*, *53*, 85–93, doi:10.1016/j.pss.2004.09.032.

- Karimabadi, H., B. Loring, H. X. Vu, Y. Omelchenko, M. Tatineni, A. Majumdar, U. Ayachit, and B. Geveci (2011), Petascale global kinetic simulations of the magnetosphere and visualization strategies for analysis of very large multi-variate data sets, in *5th International Conference of Numerical Modeling of Space Plasma Flows (ASTRONUM 2010). Proceedings of a 5th international conference held at San Diego, Calif., USA 13–18 June 2010, Astron. Soc. of the Pac. Conf. Ser.*, vol. 444, edited by N. V. Pogorelov, E. Audit, and G. P. Zank, p. 281, Astron. Soc. Pac., San Francisco, Calif.
- Karimabadi, H., et al. (2014), The link between shocks, turbulence, and magnetic reconnection in collisionless plasmas, *Phys. Plasmas*, *21*(6), 062308, doi:10.1063/1.4882875.
- Kilpua, E. K. J., Y. Li, J. G. Luhmann, L. K. Jian, and C. T. Russell (2012), On the relationship between magnetic cloud field polarity and geoeffectiveness, *Ann. Geophys.*, *30*(7), 1037–1050, doi:10.5194/angeo-30-1037-2012.
- Lavraud, B., and J. E. Borovsky (2008), Altered solar wind-magnetosphere interaction at low Mach numbers: Coronal mass ejections, *J. Geophys. Res.*, *113*, A00B08, doi:10.1029/2008JA013192.
- Lavraud, B., J. E. Borovsky, A. J. Ridley, E. W. Pogue, M. F. Thomsen, H. Rème, A. N. Fazakerley, and E. A. Lucek (2007), Strong bulk plasma acceleration in Earth's magnetosheath: A magnetic slingshot effect?, *Geophys. Res. Lett.*, *34*, L14102, doi:10.1029/2007GL030024.
- Lavraud, B., et al. (2013), Asymmetry of magnetosheath flows and magnetopause shape during low Alfvén Mach number solar wind, *J. Geophys. Res. Space Physics*, *118*, 1089–1100, doi:10.1002/jgra.50145.
- Lepping, R. P., D. B. Berdichevsky, C.-C. Wu, A. Szabo, T. Narock, F. Mariani, A. J. Lazarus, and A. J. Quivers (2006), A summary of WIND magnetic clouds for years 1995–2003: Model-fitted parameters, associated errors and classifications, *Ann. Geophys.*, *24*, 215–245, doi:10.5194/angeo-24-215-2006.
- Lin, Y., and X. Y. Wang (2005), Three-dimensional global hybrid simulation of dayside dynamics associated with the quasi-parallel bow shock, *J. Geophys. Res.*, *110*, A12216, doi:10.1029/2005JA011243.
- Lin, Y., D. W. Swift, and L. C. Lee (1996), Simulation of pressure pulses in the bow shock and magnetosheath driven by variations in interplanetary magnetic field direction, *J. Geophys. Res.*, *101*, 27,251–27,270, doi:10.1029/96JA02733.
- Lopez, R. E., C. Goodrich, M. Wiltberger, and J. Lyon (2000), Solar wind-magnetosphere energy coupling under extreme interplanetary conditions: MHD simulations, *J. Atmos. Sol. Terr. Phys.*, *62*, 865–874, doi:10.1016/S1364-6826(00)00058-4.
- Lopez, R. E., J. G. Lyon, M. J. Wiltberger, and C. C. Goodrich (2001), Comparison of global MHD simulation results with actual storm and substorm events, *Adv. Space Res.*, *28*, 1701–1706, doi:10.1016/S0273-1177(01)00535-X.
- Lopez, R. E., M. Wiltberger, S. Hernandez, and J. G. Lyon (2004), Solar wind density control of energy transfer to the magnetosphere, *Geophys. Res. Lett.*, *31*, L08804, doi:10.1029/2003GL018780.
- Lopez, R. E., V. G. Merkin, and J. G. Lyon (2011), The role of the bow shock in solar wind-magnetosphere coupling, *Ann. Geophys.*, *29*, 1129–1135, doi:10.5194/angeo-29-1129-2011.
- Luhmann, J. G., S. C. Solomon, J. A. Linker, J. G. Lyon, Z. Mikic, D. Odstrcil, W. Wang, and M. Wiltberger (2004), Coupled model simulation of a Sun-to-Earth space weather event, *J. Atmos. Sol. Terr. Phys.*, *66*, 1243–1256, doi:10.1016/j.jastp.2004.04.005.
- Matthews, A. P. (1994), Current advance method and cyclic leapfrog for 2D multispecies hybrid plasma simulations, *J. Comput. Phys.*, *112*(1), 102–116, doi:10.1006/jcph.1994.1084.
- Modolo, R., and G. M. Chanteur (2008), A global hybrid model for Titan's interaction with the Kronian plasma: Application to the Cassini Ta flyby, *J. Geophys. Res.*, *113*, A01317, doi:10.1029/2007JA012453.
- Modolo, R., G. M. Chanteur, E. Dubinin, and A. P. Matthews (2005), Influence of the solar EUV flux on the Martian plasma environment, *Ann. Geophys.*, *23*, 433–444, doi:10.5194/angeo-23-433-2005.
- Modolo, R., G. M. Chanteur, E. Dubinin, and A. P. Matthews (2006), Simulated solar wind plasma interaction with the Martian exosphere: Influence of the solar EUV flux on the bow shock and the magnetic pile-up boundary, *Ann. Geophys.*, *24*, 3403–3410, doi:10.5194/angeo-24-3403-2006.
- Němeček, Z., J. Šafránková, A. Koval, J. Merka, and L. Přeč (2011), MHD analysis of propagation of an interplanetary shock across magnetospheric boundaries, *J. Atmos. Sol. Terr. Phys.*, *73*, 20–29, doi:10.1016/j.jastp.2010.05.017.
- Omidi, N., X. Blanco-Cano, C. T. Russell, and H. Karimabadi (2004), Dipolar magnetospheres and their characterization as a function of magnetic moment, *Adv. Space Res.*, *33*, 1996–2003, doi:10.1016/j.asr.2003.08.041.
- Omidi, N., X. Blanco-Cano, and C. T. Russell (2005), Macrostructure of collisionless bow shocks: 1. Scale lengths, *J. Geophys. Res.*, *110*, A12212, doi:10.1029/2005JA011169.
- Omidi, N., D. Sibeck, X. Blanco-Cano, D. Rojas-Castillo, D. Turner, H. Zhang, and P. Kajdič (2013), Dynamics of the foreshock compressional boundary and its connection to foreshock cavities, *J. Geophys. Res. Space Physics*, *118*, 823–831, doi:10.1002/jgra.50146.
- Omidi, N., D. Sibeck, O. Gutynska, and K. J. Trattner (2014), Magnetosheath filamentary structures formed by ion acceleration at the quasi-parallel bow shock, *J. Geophys. Res. Space Physics*, *119*(4), 2593–2604, doi:10.1002/2013JA019587.
- Richer, E., R. Modolo, G. M. Chanteur, S. Hess, and F. Leblanc (2012), A global hybrid model for Mercury's interaction with the solar wind: Case study of the dipole representation, *J. Geophys. Res.*, *117*, A10228, doi:10.1029/2012JA017898.
- Rosenqvist, L., A. Kullen, and S. Buchert (2007), An unusual giant spiral arc in the polar cap region during the northward phase of a Coronal Mass Ejection, *Ann. Geophys.*, *25*, 507–517, doi:10.5194/angeo-25-507-2007.
- Šafránková, J., Z. Němeček, L. Přeč, A. A. Samsonov, A. Koval, and K. Andréevová (2007), Interaction of interplanetary shocks with the bow shock, *Planet. Space Sci.*, *55*, 2324–2329, doi:10.1016/j.pss.2007.05.012.
- Šafránková, J., M. Hayosh, O. Gutynska, Z. Němeček, and L. Přeč (2009), Reliability of prediction of the magnetosheath B_z component from interplanetary magnetic field observations, *J. Geophys. Res.*, *114*, A12213, doi:10.1029/2009JA014552.
- Shue, J.-H., et al. (1998), Magnetopause location under extreme solar wind conditions, *J. Geophys. Res.*, *103*, 17,691–17,700, doi:10.1029/98JA01103.
- Sibeck, D. G., and R.-Q. Lin (2014), Size and shape of the distant magnetotail, *J. Geophys. Res.*, *119*, 1028–1043, doi:10.1002/2013JA019471.
- Spreiter, J. R., A. L. Summers, and A. Y. Alksne (1966), Hydromagnetic flow around the magnetosphere, *Planet. Space Sci.*, *14*, 223–253, doi:10.1016/0032-0633(66)90124-3.
- Turc, L., D. Fontaine, P. Savoini, H. Hietala, and E. K. J. Kilpua (2013), A comparison of bow shock models with Cluster observations during low Alfvén Mach number magnetic clouds, *Ann. Geophys.*, *31*, 1011–1019, doi:10.5194/angeo-31-1011-2013.
- Turc, L., D. Fontaine, P. Savoini, and E. K. J. Kilpua (2014a), A model of the magnetosheath magnetic field during magnetic clouds, *Ann. Geophys.*, *32*, 157–173, doi:10.5194/angeo-32-157-2014.
- Turc, L., D. Fontaine, P. Savoini, and E. K. J. Kilpua (2014b), Magnetic clouds' structure in the magnetosheath as observed by Cluster and Geotail: Four case studies, *Ann. Geophys.*, *32*, 1247–1261, doi:10.5194/angeo-32-1247-2014.
- von Alfthan, S., D. Pokhotelov, Y. Kempf, S. Hoilijoki, I. Honkonen, A. Sandroos, and M. Palmroth (2014), Vlasiator: First global hybrid-Vlasov simulations of Earth's foreshock and magnetosheath, *J. Atmos. Sol. Terr. Phys.*, *120*, 24–35, doi:10.1016/j.jastp.2014.08.012.

- Walker, A. D. M. (1981), The Kelvin-Helmholtz instability in the low-latitude boundary layer, *Planet. Space Sci.*, *29*, 1119–1133, doi:10.1016/0032-0633(81)90011-8.
- Wang, X. Y., Y. Lin, and S.-W. Chang (2009), Hybrid simulation of foreshock waves and ion spectra and their linkage to cusp energetic ions, *J. Geophys. Res.*, *114*, A06203, doi:10.1029/2008JA013745.
- Yan, M., and L. C. Lee (1996), Interaction of interplanetary shocks and rotational discontinuities with the Earth's bow shock, *J. Geophys. Res.*, *101*, 4835–4848, doi:10.1029/95JA02976.
- Yermolaev, Y. I., N. S. Nikolaeva, I. G. Lodkina, and M. Y. Yermolaev (2012), Geoeffectiveness and efficiency of CIR, sheath, and ICME in generation of magnetic storms, *J. Geophys. Res.*, *117*, A00L07, doi:10.1029/2011JA017139.
- Zhang, J., M. W. Liemohn, J. U. Kozyra, B. J. Lynch, and T. H. Zurbuchen (2004), A statistical study of the geoeffectiveness of magnetic clouds during high solar activity years, *J. Geophys. Res.*, *109*, A09101, doi:10.1029/2004JA010410.